PCCP

PAPER

View Article Online
View Journal | View Issue

Check for updates

Cite this: *Phys. Chem. Chem. Phys.*, 2018, **20**, 8228

Molecular dynamics simulation on the mechanical properties of natural-rubber-*graft*-rigid-polymer/rigid-polymer systems†

Meng Wei, Pengxiang Xu, Yizhong Yuan,* Xiaohui Tian,* Jinyu Sun and Jiaping Lin

A coarse-grained model-based molecular dynamics simulation was employed to investigate the mechanical properties of NR-*graft*-rigid-polymer/rigid-polymer systems (N_{30}-*g*-$(R_3)_6/R_{10}$). An external factor (the strain rate) as well as internal factors such as the nonbonding interaction strength, the proportion of rigid polymers, and architecture parameters (the length and number of graft chains in a molecule) were examined for their effect on the tensional behavior of N_{30}-*g*-$(R_3)_6/R_{10}$ systems. Simulation results show that a higher strain rate can promote the enhancement of mechanical performance, such as a higher modulus or yield stress. Moreover, the stress and modulus increase with an increase of the nonbonding interaction strength within rigid polymers or of the rigid polymer proportion in the systems. However, the increasing stress was found to reach a limit with a continuously increasing rigid polymer proportion. On increasing the number of graft chains in a molecule, the stress increases at small strains. However, at large strains, the evident increase in stress was found in systems in which a graft molecule has longer graft chains. In addition, our research shows that N_{30}-*g*-$(R_3)_6/R_{10}$ blends exhibit improved mechanical properties and better compatibilities relative to N_{30}/R_{10}, which is consistent with the experimental results. Lastly, comparisons with experimental observations were also made to ensure the rationality of the simulation results. Overall, bond stretching, bond orientation, and nonbonding interactions were found to be crucial in governing the mechanical properties of the N_{30}-*g*-$(R_3)_6/R_{10}$ systems. These findings may provide important information for further experimental and simulation studies of NR hybrid materials.

Received 20th November 2017,
Accepted 16th February 2018

DOI: 10.1039/c7cp07807b

rsc.li/pccp

1. Introduction

Natural rubber (NR) latex, containing 93–95 wt% *cis*-1,4-polyisoprene, has been extensively utilized in the fabrication of dipping goods because of its good film-forming ability, tensile strength and resilience.[1] However, NR latex lacks mechanical strength and oxidation resistance due to the lithe chains and the presence of the carbon–carbon double bonds in the structure.[2] To broaden industrial applications, blending NR with rigid polymers has been studied extensively, and there is a clear drive towards films of an elastomeric matrix containing high-modulus inclusions, which provide good mechanical properties for latex blends.[3–5] However, the components are highly incompatible and immiscible in blends due to the mismatch of polarity and hydrophilicity.[6] Increasing the compatibilization of the immiscible pairs is a promising strategy for property improvement of the blends because it can achieve good dispersions in rigid materials.[7,8] Many promising studies have shown that by the addition of a rigid copolymer of NR, which works as a compatilizer to interact with both blend components, one can obtain enhanced mechanical properties.[3–5,9,10]

Recently, blends of NR latex and poly(methyl methacrylate) (PMMA) have exhibited both the excellent mechanical characteristics of PMMA and the elastic properties of NR.[11] Most studies regarding latex blends focus on the compatibilization and the phase behavior of the blend components.[1,12,13] For example, Oommen *et al.*[14] reported the incorporation of NR-*g*-PMMA into the heterogeneous NR/PMMA blend as a compatibilizer. The NR-*g*-PMMA parts could effectively reduce the interfacial tension between the two different phases and improve the properties of the blend. Jayasuriya *et al.*[11] have studied an interpenetrating polymer network (IPN) which can be obtained from the *in situ* polymerization of MMA in the NR films. The formation of many

Key Laboratory for Ultrafine Materials of Ministry of Education and Shanghai Key Laboratory of Advanced Polymeric Materials, School of Materials Science and Engineering, East China University of Science and Technology, Shanghai 200237, China. E-mail: yizhongyuan2004@hotmail.com, tianxh@263.net

† Electronic supplementary information (ESI) available: Details on model construction and the effects of external and internal factors on the mechanical properties. See DOI: 10.1039/c7cp07807b

chemical interactions and crosslinks between the PMMA chains and NR chains was clearly presented. Nakason *et al.*[15] revealed that the morphology of an epoxidized natural rubber (ENR) and PMMA blend steadily becomes smooth when the ENR content increases. However, until now systematic analysis of the mechanical properties of blend latex is still limited. Few primary investigations revealed that the blend systems possess enhanced mechanical properties. For example, Collins and Gorton[16] incorporated a certain amount of MG49 latex to increase the modulus of NR thread. Gorton[17] added MG49 latex to NR to improve the tear strength and puncture strength of NR. Due to the limitations of experimental technology and the structural complexities of NR blend polymers, there is still a lack of in-depth insight into the interacting structure within the blends, the packing of components and the mechanism of the effects on the mechanical properties.

In addition to the experiments, simulation approaches such as finite-element methods based on fluid mechanics (FEMBFM),[18] the lattice Boltzmann method (LBM),[19] and molecular dynamics (MD),[20,21] have been applied to study the interactions and dispersion of components in particle-graft polymer/polymer blends. Jiang[22] and coauthors studied the effects of variation of structure and interaction strength on the mechanical behavior of blends of polymers and nanoparticles. The results showed that the mechanical properties were enhanced with increasing nanoparticle–polymer interaction or increasing nanoparticle size. In relation to property evaluations, MD simulations are powerful tools to gain insight into the mechanical properties of polymer based composites,[23–30] and have been broadly employed in studies of the mechanical properties of polymer blend systems. Xiao[31] investigated the mechanical properties of blends of 1,3,5-triamino-2,4,6-trinitrobenzene (TATB) and fluorine polymers, which can be effectively improved by adding appropriate amounts of the polymers. Cho *et al.*[25] found that decreasing the particle size results in an enhanced Young's moduli by studying the influence of nanoparticle size on the elastic properties of nanoparticle/polymer blends in bulk. Liu *et al.*[32] preliminarily revealed the reinforcement mechanisms of rubber by adopting idealized models of polymer networks and nanoparticles and investigating the dependency of the stress–strain behavior on nanoparticle amount, nanoparticle size and nanoparticle–rubber interaction. However, little attention until now has been paid to the mechanical properties of NR blend systems by a MD method.

The purpose of this study is to investigate the effects of various factors on the mechanical properties of NR-*graft*-rigid-polymer/rigid-polymer blends using molecular dynamics simulations. This provides a way to get a deeper insight into the mechanism, which is difficult to study experimentally due to the limitations of experimental methodology and the difficulties of studying the principle factors affecting the mechanical properties in NR-*graft*-rigid-polymer/rigid-polymer systems.

By systematically varying the strain rate, interaction strength, architecture parameters and the rigid polymer proportion of NR-*graft*-rigid-polymer/rigid-polymer blends, we identify clear trends in the mechanical properties with reinforcement of our systems. The simulation results show that the mechanical properties can be enhanced by increasing strain rate, interaction strength, or the proportion of the rigid polymer in the blends. However, too short graft chains and too few graft chains both weaken the mechanical properties. A comparison of the mechanical properties among NR-*graft*-rigid-polymer/rigid-polymer blends, neat polymers, and rigid-polymer/NR blends was made. Such simulated results were also compared with the available experimental observations. By taking into account the external and internal factors during the deformation process of the systems, we established the relationship between these influencing factors and the mechanical properties. These correlations can offer useful information for further experimental and simulation studies of NR hybrid materials.

2. Methods and models

2.1. Structure construction

In order to explore the mechanical properties and morphologies of NR-*graft*-rigid-polymer/rigid-polymer blends, a model of an NR-*graft*-rigid-polymer chain was first constructed. Natural rubber (NR) contains almost 95 wt% *cis*-1,4-polyisoprene flexible chains, which is the main contributor to the mechanical properties of NR.[33] Thus we can simplify the model of NR by only considering *cis*-1,4-polyisoprene irrespective of the minority components. A coarse-grained model was constructed[34] as shown in Fig. 1. The polymers were constructed as linear chains with different sizes for the different polymers, where the size is denoted by the number of polymer beads. We use N_{30}-*g*-$(R_3)_6/R_{10}$ to represent the NR-*graft*-rigid-polymer/rigid-polymer blend systems, where N and R stand for the NR matrix and the rigid-polymer beads, respectively. By setting the unit length of the polymer beads to σ, and the masses of the polymer beads to m, we adjust the density of the rigid polymer bead to that of an NR bead. The initial structure of the molecule was constructed in a box with initial lengths of 100 by randomly positioning the NR beads in the unit box and generating NR chains bead by bead with a fixed distance. The method can be considered as a modified version of the conventional self-avoiding random walk (SARW) technique.[35] Rigid polymer chains were described in a similar way, whereas the graft rigid chains started from the fixed grafting sites (the number of graft chains was set to 6 in a molecule) and had the same length. We set the lengths of the

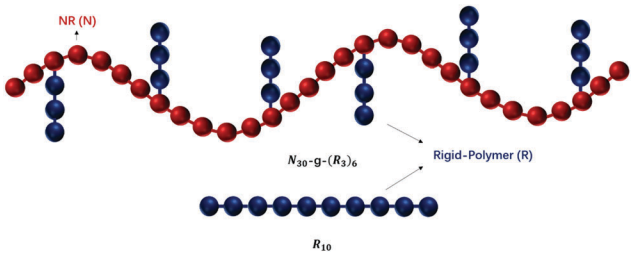

Fig. 1 Model of NR-*graft*-rigid-polymer/rigid-polymer blend systems N_{30}-*g*-$(R_3)_6/R_{10}$. The red and blue beads represent NR polymers and rigid polymers, respectively. A harmonic angle potential was adopted for the rigid polymers. $(R_3)_6$ stands for 6 graft chains each with 3 rigid polymer beads.

NR matrix, rigid graft chain and rigid chain to 30, 3 and 10, respectively.

The coarse-grained model, which simulates large polymer systems or long polymeric processes by setting "pseudo-atoms" to represent groups of atoms, is an efficient method to compromise between computational costs and efficiency compared to traditional all atom methods which require large computer resources to explicitly represent every atom of the system. Only if the traits of the polymer chains and the practical structure are established in detail can the coarse-grained model be used to simulate larger length scales and longer time scales, which is extensively utilized for macromolecular systems.[36,37]

In our simulation model, 9000 polymer beads in total[38] were constructed to represent the NR polymers and rigid polymers, with each polymer bead representing a mass of monomers. By varying the number of polymer chains, polymer beads for each polymer type were evenly separated. Periodic boundary conditions were employed to replicate the unit box in three dimensions, and thus this model can be regarded as the unit extended infinitely. In our model, the blend systems we investigated are in a rubbery state irrespective of the entanglement effects of the polymer chains.[39] Modeling procedures in which one tunes the parameters to match experimental data to reveal the dynamic and static behavior of the polymer chains are also widely adopted in the literature.[38,40]

2.2. Potential function

Once the molecular structures were set up, corresponding particle interactions were then described using potential functions. In our model, the NR was described by appropriate bonding stretching potentials while angle bending potentials were also utilized to describe the rigid chains, which is referred to as bonded potential. The nonbonding van der Waals interactions between any pair of beads were given by the standard 12/6 Lennard-Jones (LJ) potential U_r:

$$U_r = \begin{cases} 4\varepsilon\left[\left(\frac{\sigma}{r}\right)^{12} - \left(\frac{\sigma}{r}\right)^{6}\right], & r < r_c \\ 0, & r \geq r_c \end{cases} \quad (1)$$

where r_c is the cutoff distance and ε is the strength parameter between polymer beads. The intermolecular attraction or repulsion can be adjusted by the cutoff distance r_c (pure repulsion when $r_c \leq 2^{1/6}$ and containing attraction when $r_c > 2^{1/6}$), which can be seen in Fig. S1 (ESI†). By choosing appropriate ε and r_c values for polymer beads, we can specify the intermolecular interactions between different polymer beads.[41] In the present work, the interactions within each polymer type are truncated at an attractive cutoff distance, namely $r_c = 2.5$, according to Lin's work;[42] however, we set $r_c = 2^{1/6}$ for the interaction between rigid polymers and NR, which is a repulsive cutoff for the rigid polymer beads and NR beads. Such a scheme of interactions between different polymer types is to match the experimental evidence that blending the rigid polymers with NR latex is hard due to the different polarities.[12] The attraction is to ensure a positive thermal expansion coefficient within each polymer type.[43] The strength of intermolecular interactions can be tuned by the strength parameter, ε (ε_{NN}, ε_{RR} and ε_{NR} were used to denote the interaction within NR polymer beads, the interaction within the rigid polymer beads and the interaction between the NR and rigid polymer beads, respectively). We can investigate the effect of the intermolecular interactions of the rigid polymers on the mechanical properties and morphologies by varying the strength parameter between the rigid polymers ε_{RR}. For the purpose of studying various rigid polymers, this means that the study does not focus on a specific rigid material. The interaction parameters ε_{NN} (within NR) and ε_{NR} (between NR and rigid polymer beads) were set to be fixed, where NR can be relatively treated as a soft material. Therefore, ε_{RR} is chosen to be 1.0, 2.5, 5.0 and 10.0 to represent different rigid polymers according to Jiang's studies[22] and $\varepsilon_{NN} = 1.0$ is selected for NR. In addition, the interaction between NR and the rigid polymer beads, namely ε_{NR}, is chosen to be 5.0, which provides a strong repulsion between NR and the rigid polymers.[6]

The interaction between the adjacent bonded polymer beads is expressed by the modified finite extensive nonlinear elastic (FENE) potential:[32]

$$U_{FENE} = -0.5kR_0^2 \ln\left[1 - \left(\frac{r}{R_0}\right)^2\right] \quad (2)$$

such potential is used for molecules with rigid bonds as a bead-spring model and can even produce mechanical properties in small deviations. The spring constant of FENE bonds has the ability to restrict the bond stretching, and thereby influences the mechanical properties in terms of conformational entropy and provides a more physical behavior. k is a parameter to determine the strength of interaction between polymer beads and R_0 is fixed for convenience. Therefore, $k = 30$ is selected for NR, which is just enough to avoid chain crossing, and k is relatively chosen to be 50 for the rigid polymers according to the studies of Kremer and Grest.[44] In view of the stiffness or rigidity of the rigid polymers relative to the flexible NR, a harmonic angle potential is also adopted:

$$E = K(\theta - \theta_0)^2 \quad (3)$$

where θ_0 is the equilibrium value of the angle and K is a parameter describing the strength of interaction within angles. Because of the coarse-grained beads, $\theta_0 = 180°$ is selected for the rigid polymer interaction. Through tuning the parameters k in FENE and K in the harmonic angle potential, different rigid polymers can be obtained. However, the bending factor is not our goal in this work, and consequently we set K to be a constant for convenience.

In our model, all quantities adopted reduced units and the units of mass, length and energy are defined by m, σ and ε, respectively. The time unit τ is defined as $\tau = (m\sigma^2/\varepsilon)^{1/2}$, which can be converted into the real unit by matching the simulated lateral diffusion coefficient to the experimentally measured value.[42]

2.3. Simulation details

Our MD simulations were performed using LAMMPS,[45] which was developed by Sandia National Laboratories. All simulations

were carried out at the same temperature T of 1.0 with a time step $\Delta t = 0.004\tau$ (τ denotes the unit time). The mechanical properties of the N_{30}-g-$(R_3)_6/R_{10}$ blends were investigated by performing in two steps the equilibrium and the non-equilibrium processes.

2.3.1 Equilibrium simulation. In the equilibrium process, the velocity-Verlet algorithm[35] was used to integrate the equation of motion. The polymer chains naturally diffused in *NVT* ensemble where the large volume size of the simulation cell was specified so that the molecules had enough space and kinetic energy for free diffusion and interaction. Because initial overlaps existed between polymer beads, a soft repulsive potential was adopted:[46]

$$U_{\text{soft}} = \begin{cases} A\left[1+\cos\left(\frac{\pi r}{\sqrt[6]{2}\sigma}\right)\right], & r \le \sigma \\ 0, & r > \sigma \end{cases} \quad (4)$$

where the coefficient $A = 20.0$. After 10 000 steps of removing overlap procedures, we compressed the initial box to a volume fraction of 0.45.[47] Because the initial box and the number of total polymer beads were the same for all blend systems, the volume fraction was approximately the same for each system. The equilibrated molecular structure with minimized energy was then accomplished by performing the *NPT* ensemble where $P = 0$ and $T = 1.0$ were adopted using the Nosé–Hoover barostat and thermostat.[48] To achieve the equilibrium state of the systems, 5×10^7 steps were carried out to ensure enough computing time. The temporal evolutions of the morphologies and the total energy of the systems were also examined (see Fig. S2, ESI†). It was found that the total energy drops first and then maintains a constant value with little fluctuation. After 1×10^7 steps, the total energy is stabilized and the morphology is not changed (insets of Fig. S2, ESI†), and thus it can be considered that the systems have reached equilibrium for a relatively long time.

2.3.2 Nonequilibrium simulation. After reaching the equilibrium state, in the next step, a nonequilibrium simulation is employed to simulate tensile tests which were carried out by deforming the cubic simulation box to a cuboid one under the *NVT* ensemble with $\Delta t = 0.001\tau$ and $T = 1.0$ according to the research of Mark and of Xu.[47,49] The box is elongated in the z-direction and compressed in the x-direction and y-direction, while the box volume is invariable. The particles in the box move in the z-direction following the deformation of the simulation box. Note that, the definition of stress is different from that in the continuum mechanics framework as it is supposed that the materials have no volume change and are incompressible.[48] In our simulation, a constant engineering strain rate was employed during the tensional process. This means the box dimension changes linearly with time from its original to final length value in one dimension. Tensile strain is defined as $\Delta l/l_0$, where l_0 is the original box length and Δl is the change relative to the original length l_0. The strain rate was mostly set as $0.2\tau^{-1}$, which is comparable with the segmental relaxation.[50] The tensile stress σ in the z-direction can be calculated from the deviatoric part of the stress tensor:[51]

$$\sigma = (1+\mu)(-P_{zz}+P) = 3(-P_{zz}+P)/2 \quad (5)$$

where μ is the Poisson's ratio and was set to 0.5[49] and $P = \sum_i P_{ii}/3$ is the hydrostatic pressure. P_{ii} is the diagonal component of the pressure tensor, which is the negative value of the virial stress σ_{ii} in the i-direction, and σ_{ii} is defined as:[12]

$$\sigma_{ii} = -\frac{1}{V}\sum_{\alpha}\left(M^{\alpha}v_i^{\alpha}v_i^{\alpha} + \frac{1}{2}\sum_{\beta\neq\alpha}F_i^{\alpha\beta}r_i^{\alpha\beta}\right) \quad (6)$$

where V is the volume of the MD unit cell; M^{α} is the mass of atom α; v_i^{α} is the i-component of the velocity of atom α; $F_i^{\alpha\beta}$ is the i-component of the force between atoms α and β; and $r_i^{\alpha\beta}$ is the i-component of the distance between atoms α and β. Here, the first term is associated with the contribution from kinetic energy resulting from the change in potential energy due to the applied deformation.

3. Results and discussion

In this work, we mainly investigate the external and internal effects on the mechanical properties of N_{30}-g-$(R_3)_6/R_{10}$ systems. The strain rate was the external factor, whereas the nonbonding interaction strength, rigid polymer proportion, and architecture parameters like the length of and the number of graft chains of an N_{30}-g-$(R_3)_6$ molecule were treated as internal factors. Moreover, we constructed models to make a comparison of the properties of the blend of NR-*graft*-rigid-polymer and rigid polymer, the blend of NR and rigid polymer, and pure NR, namely N_{30}-g-$(R_3)_6/R_{10}$, N_{30}/R_{10} and N_{30}. At last comparisons with experimental observations were made to provide the rationality of our models.

In our work, some parameters which were beyond our study scope were fixed, such as the interaction strength within NR, $\varepsilon_{NN} = 1.0$, the interaction strength between NR and the rigid polymers, $\varepsilon_{NR} = 5.0$, and the total number of polymer beads of 9000 and $T = 1.0$, *etc.* More details can be seen in the previous section. Furthermore, we study each influential factor or parameter by keeping other factors or parameters invariable. Instead of choosing the optimal parameters, we select the ones with more stable results to study the effects of another factors or parameters on the mechanical properties, which gives us more credible results.

3.1. External effect of strain rate on the mechanical properties of the N_{30}-g-$(R_3)_6/R_{10}$ blend systems

In this subsection, we display the stress–strain curves with different strain rates, varying from $0.1\tau^{-1}$ to $0.5\tau^{-1}$, as well as the extracted features like tensional modulus and yield stress, which are shown in Fig. 2. The systems contain 80% rigid polymer beads and $\varepsilon_{RR} = 5.0$. Each graft molecule has 6 graft chains with a length of 3. The mechanical properties of the blends were obtained by performing uniaxial tension at a set strain rate, which is repeated ten times with uncorrelated initial polymer structures. Such an approach provides the error bars as well as a statistical average to the noisy, which is unavoidable in MD simulations.

As can be seen in Fig. 2a, the stress rises rapidly at small strain and ascends with increasing strain rate at the same strain.

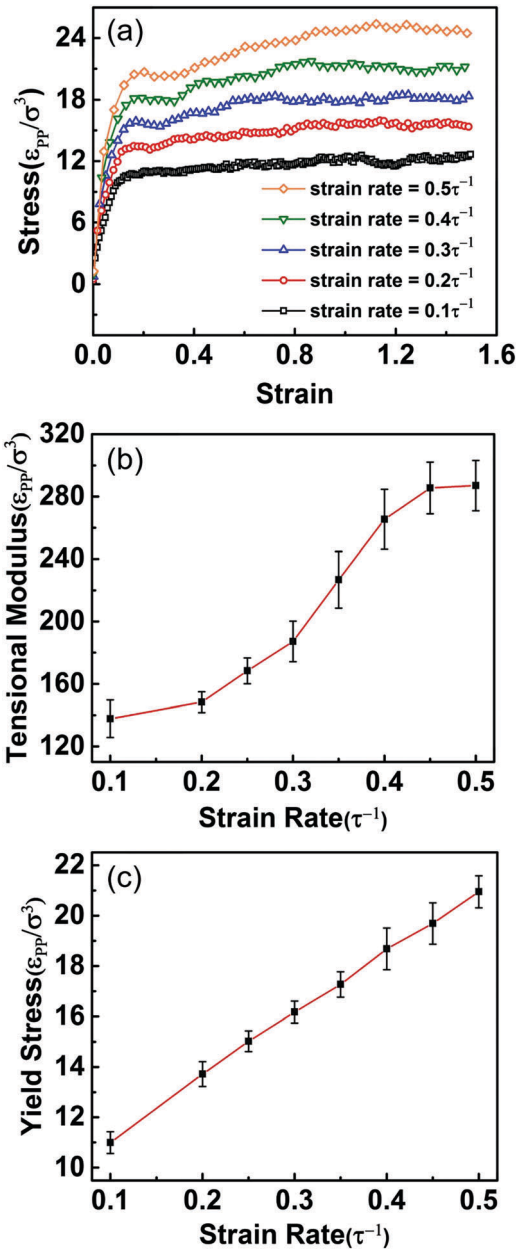

Fig. 2 (a) Stress–strain curves for various strain rates in the N_{30}-g-$(R_3)_6$/R_{10} systems at ε_{RR} = 5.0. (b) Tensional modulus as a function of strain rate in the N_{30}-g-$(R_3)_6$/R_{10} systems. (c) Yield stress *versus* strain rate in the N_{30}-g-$(R_3)_6$/R_{10} systems.

Furthermore, as the strain increases, a larger increase in stress was found at higher strain rates, while the stress barely changes at lower strain rates. Fig. 2b shows the tensional modulus E as a function of strain rate, which was derived from the slope of the stress–strain curve within 2% strain.[25] E increases with increasing strain rate, and when the strain rate is less than $0.4\tau^{-1}$, E escalates with an increasing slope, while at excessively large strain rate the increment in E is moderated. This indicates that a higher strain rate results in better mechanical properties, however, one cannot expect that the tensional modulus can be continuously elevated by an infinitely increasing strain rate. The plot of yield stress *versus* strain rate (see Fig. 2c) shows that the yield stress increases linearly with increasing strain rate, suggesting that the materials exhibit a better mechanical performance at larger strain rates.

In this work, the bond orientation P_2, the effective bond length $l_{b,eff}$, and the change of nonbonding potential ΔE were extracted to study the microscopic origin of the distinct mechanical properties in tensile processes. In general, the generated tensile stress arises from the loss of conformational entropy and the increase of interaction enthalpy.[52,53] The loss of conformational entropy is characterized by $l_{b,eff}$ and P_2. The $l_{b,eff}$ was computed as the average length for all bonds. Fig. 3a shows that $l_{b,eff}$ increases significantly with increasing strain in the smaller strain region and then tends to increase more slowly or even decrease in the larger strain region. At the same strain, the value of $l_{b,eff}$ was found to be larger with higher strain rates, indicating that with a faster tensile speed the degree of bond stretching is larger. On the one hand, at the same strain the systems obtain more kinetic energy due to the higher strain rate and the increased energy leads to stronger stretching of the bonds in systems with a higher strain rate. On the other hand, chain relaxation will weaken the bond stretching during the tensile process. A higher strain rate leads to a weaker effect of chain relaxation, which causes a decrease in the decay of bond stretching and therefore the systems exhibit stronger bond stretching. During the tensile process $l_{b,eff}$ gradually becomes constant. Note that the

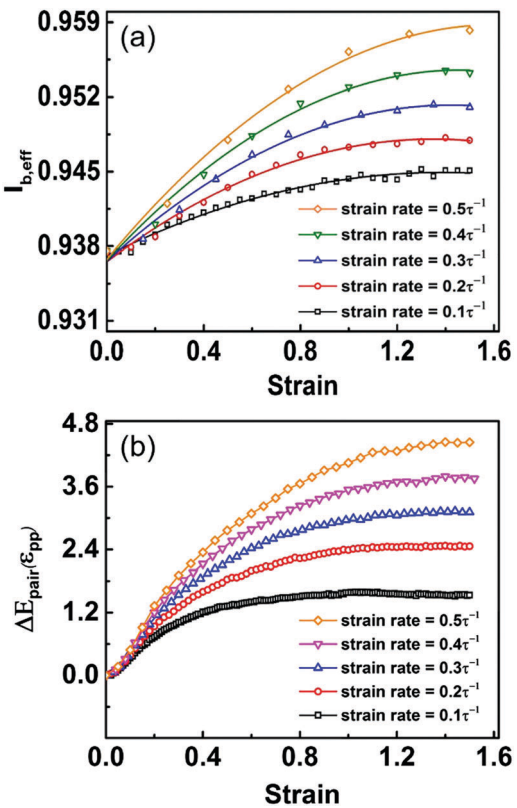

Fig. 3 (a) Effective bond length $l_{b,eff}$ *versus* strain for various strain rates. (b) ΔE_{pair} with respect to strain at different strain rates for N_{30}-g-$(R_3)_6$/R_{10} blends.

value of $l_{b,eff}$ becomes stable faster at lower strain rates. P_2 is given by $(3\langle\cos^2\theta\rangle - 1)/2$,[43] where θ denotes the angle between a given bond and the deformation direction. The possible values of P_2 range from −0.5 to 1, and values of −0.5, 1 and 0 represent orientations perpendicular to the reference direction, parallel to the reference direction, or randomly oriented, respectively. P_2 was found to increase during the tensile process (see Fig. S3, ESI†). However, the values of P_2 are almost the same at various strain rates but become a little larger with increasing strain rate at the same strain, indicating that bond orientations have similar behavior during the tensile process at different strain rates. By studying the change of $l_{b,eff}$ and P_2 during the tensile processes we can characterize bond stretching and chain alignment, respectively.

The contributions from interaction enthalpy can be manifested by the change of nonbonding potential ΔE_{pair}, which is the difference of the total nonbonding potentials between the deformed and undeformed state. This is the main source of the increase in energy during the tensile process. As can be seen in Fig. 3b, ΔE_{pair} increases with increasing strain, and the rate of increase of ΔE_{pair} can be decreased swiftly by increasing the strain or decreasing the strain rate. This suggests that interaction enthalpy contributes more to the increase in mechanical properties at smaller strains with a higher strain rate. We can also see that ΔE_{pair} is larger in the systems with higher strain rates, which means that nonbonding interactions make a great contribution to the enhanced mechanical properties.

3.2. Effect of internal factors on the mechanical properties of N_{30}-*g*-$(R_3)_6/R_{10}$ systems

In this subsection, we investigate the effect of internal factors on the mechanical properties of N_{30}-*g*-$(R_3)_6/R_{10}$ blends. In order to characterize the important effect of interaction strength within the rigid polymer beads on the mechanical properties of N_{30}-*g*-$(R_3)_6/R_{10}$ blends, the strength parameters of both intermolecular interaction and intramolecular interaction were taken into account. On the one hand, by changing the nonbonding strength parameter, ε_{RR}, from 1.0 to 10.0 we examined the effect of intermolecular interaction strength. On the other hand, we studied the intramolecular interaction strength through varying the bonded strength parameter k in FENE potentials. We can see that the tensile behavior in systems with different intramolecular interactions is nearly the same but noisy (see Fig. S4, ESI†), indicating that the mechanical properties are not mainly determined by the intramolecular interaction but by the intermolecular interaction, which is reasonable.

As can be seen in Fig. 4a, the tensional modulus was derived at strain rate of $0.2\tau^{-1}$, which increases with increasing nonbonding interaction strength between rigid polymers. The dashed line indicates the tensional modulus of the neat NR polymers. However, the tensional modulus at ε_{RR} = 1.0 is lower than that of pure NR, suggesting that the mechanical properties of the blend of NR-*graft*-rigid-polymer and rigid polymer can only be enhanced by adding a rigid polymer with a stronger nonbonding interaction. The typical morphology snapshots at ε_{RR} = 1.0, 2.5, 5.0 and 10.0 are shown in the insets. Moreover, it shows that the larger the intermolecular interaction strength is, the worse the compatibility of the blend systems, which is

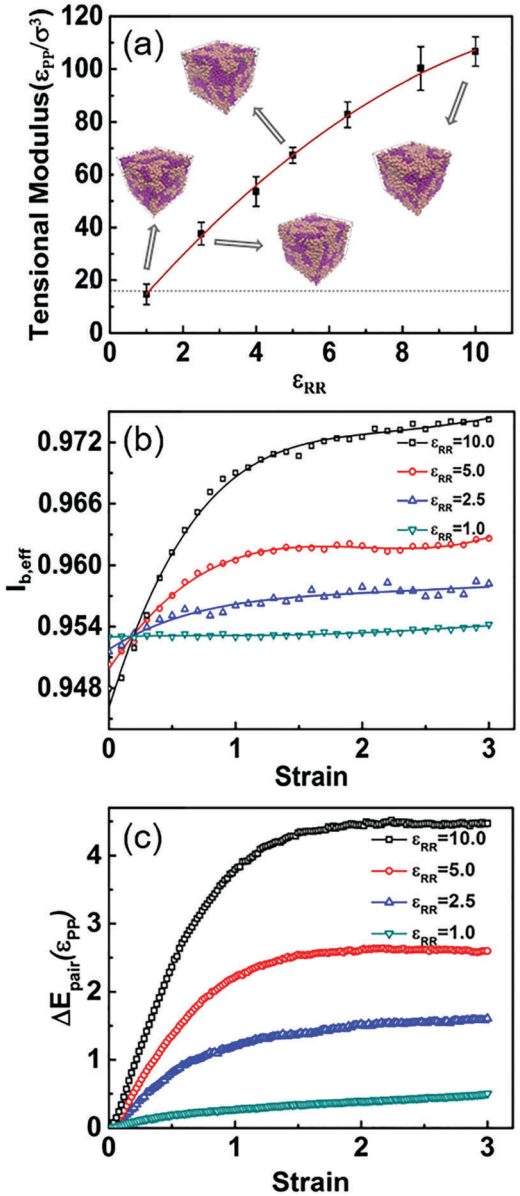

Fig. 4 (a) Tensile modulus as a function of ε_{RR} for N_{30}-*g*-$(R_3)_6/R_{10}$ systems. The dashed line indicates the tensile modulus of the neat NR polymer. The insets show typical morphology snapshots at ε_{RR} = 1.0, 2.5, 5.0 and 10.0. The rigid polymers are denoted with purple beads. (b) Effective bond length $l_{b,eff}$ *versus* strain for various ε_{RR}. (c) ΔE_{pair} as a function of strain for N_{30}-*g*-$(R_3)_6/R_{10}$ blends at different ε_{RR} values.

reasonable because the differences between NR and the rigid polymer become greater as rigid polymers with stronger intermolecular interactions are added. Additionally, the representative stress–strain curves of the N_{30}-*g*-$(R_3)_6/R_{10}$ blends at various ε_{RR} values are shown in Fig. S5a (ESI†). As ε_{RR} increases, the stress increases rapidly at the same strain, and rises more significantly at larger strain.

The dependence of tensile behavior on ε_{RR} can be explained by the effective bond length, bond orientation, and change of nonbonding potential. $l_{b,eff}$ and ΔE_{pair} as a function of strain for various ε_{RR} values are shown in Fig. 4b and c, respectively.

As the strain increases, the value of $l_{b,eff}$ increases gradually, although it only increases slightly at $\varepsilon_{RR} = 1.0$, which means the bonds stretch more during the tensile process. Furthermore, $l_{b,eff}$ increases more evidently with growing ε_{RR} at small strains, and still ascends at large strains in systems with larger ε_{RR}. This suggests that the degree of bond stretching increases notably for larger ε_{RR}. On the one hand, a larger ε_{RR} makes the systems much harder to extend and so a stronger tensile force is needed to stretch the systems to the same length. Therefore, systems with larger ε_{RR} values obtain more energy from the stronger tensile force, which results in more obvious bond stretching. On the other hand, the chain relaxation is weaker in systems with larger ε_{RR} values due to stronger intermolecular attraction, which reduces the decrease of bond stretching. However, at small strains $l_{b,eff}$ was found to be smaller for larger ε_{RR} values because of the stronger attraction between rigid polymers. The values of bond orientation P_2 increase with increasing strain, but are almost the same at various ε_{RR} values at the same strain, and this is plotted in Fig. S5b (ESI†). The contribution from interaction enthalpy, namely the change of nonbonding potential, is shown in Fig. 4c. ΔE_{pair} increases rapidly to a plateau as the strain increases, and then has little changes at larger strains. With increasing ε_{RR}, ΔE_{pair} has a larger increase during the whole tensile process, suggesting that systems with stronger nonbonding interactions have larger enthalpy gains. Greater bond stretching and a larger increase in the change of nonbonding potential provide a higher entropy loss and enthalpy gain in systems with higher ε_{RR} values, which cooperatively contribute to the larger stress and modulus. Note that in systems with $\varepsilon_{RR} = 10.0$, the continuous increase in $l_{b,eff}$ results in a continuously increasing stress at larger strains as shown in Fig. 4b and Fig. S5a (ESI†). This suggests that the increase in stress at larger strains is mostly contributed to by entropy loss.

We studied the mechanical properties of N_{30}-g-$(R_3)_6/R_{10}$ blends with various proportions of rigid polymers at $\varepsilon_{RR} = 5.0$ and a strain rate of $0.2\tau^{-1}$. As shown in Fig. 5a, the tensional modulus E increases gradually as the proportion of rigid polymer increases. From the insets, the morphologies of the blends show that as the proportion of rigid polymer increases, the rigid polymers come to dominate the blends. The yield strain was found to decrease when the proportion of rigid polymer increases (see Fig. 5b). Moreover, by changing the proportion of rigid polymer from 50% to 80%, we find that the stress increases continuously at the same strain (see Fig. S6a, ESI†). This indicates that the mechanical properties of the blends are dominated by the rigid polymers, which possess relatively higher tensile stress and modulus values. Moreover, when the proportion of rigid polymer further increases to 80%, the stress curve flattens out and overlaps with that of the blend with a 75% rigid proportion. The result suggests that saturation of enhanced performance can be found when one attempts to improve the mechanical properties of N_{30}-g-$(R_3)_6/R_{10}$ blends by continually adding rigid polymers.

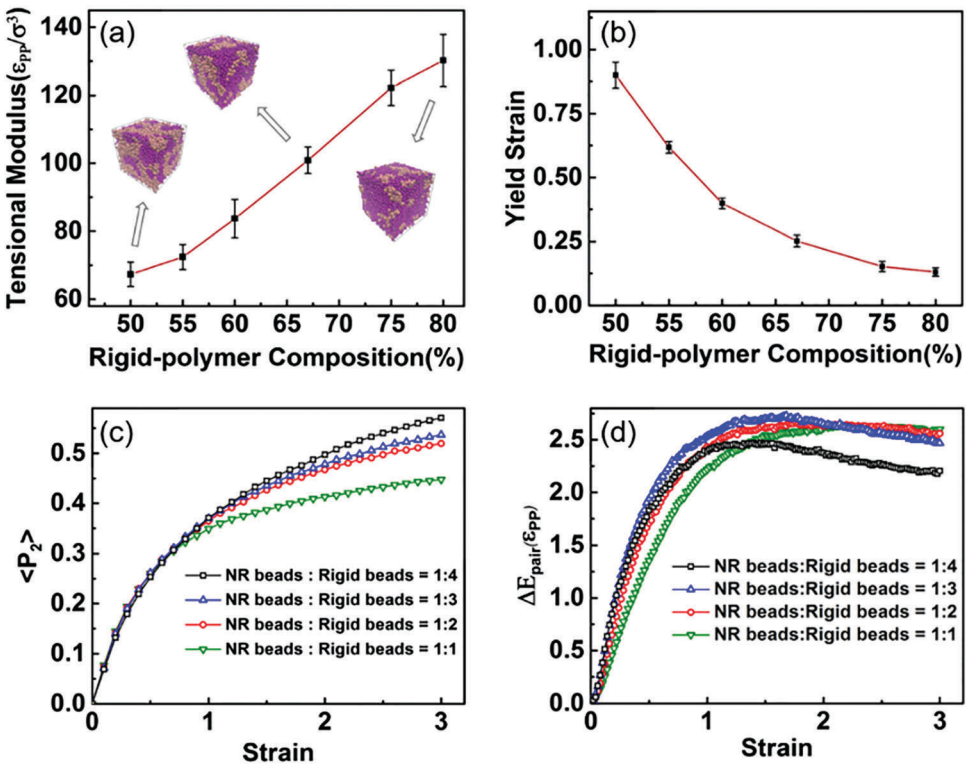

Fig. 5 (a) Tensional modulus with respect to rigid polymer proportion for N_{30}-g-$(R_3)_6/R_{10}$ systems. The insets show typical morphology snapshots at 50%, 75% and 80% rigid polymer proportion, in which the rigid polymers are denoted with purple beads. (b) Curve of yield strain *versus* rigid polymer proportion. (c) Bond orientation P_2 with respect to strain for various ratios of NR beads to rigid beads. (d) ΔE_{pair} as a function of strain for N_{30}-g-$(R_3)_6/R_{10}$ systems at different ratios of NR beads to rigid beads.

The mechanical properties were explained by the bond orientation, effective bond length and the interaction potential. From Fig. 5c, it can be seen that P_2 has almost the same value at small strains for different rigid proportions, while at large strain the values of P_2 become larger in systems with a larger proportion of rigid polymer, indicating that the systems with more rigid polymer have a greater degree of bond orientation during the tensile process. However, systems with a larger rigid proportion exhibit a smaller degree of bond stretching resulting from the smaller value of the $l_{b,eff}$ at the same strain as shown in Fig. S6b (ESI†). This means that stronger attraction between the numerous rigid polymer beads makes the average bond length shorter. Additionally, $l_{b,eff}$ changes little at large strains. Fig. 5d shows that the change of nonbonding potential increases rapidly at small strains and has slight changes at large strains, and declining trends of ΔE_{pair} were even found in systems with more than 66% rigid polymer at large strains. This suggests that the nonbonding potential mainly contributes to the increase in stress at small strains.

Under the cooperative effects of entropy and enthalpy, the behaviors of the tensile process are formed (see Fig. 5a and b and Fig. S6a, ESI†). In the small strain region, the increase in stress is contributed to by both enthalpy gain (increase in ΔE_{pair}) and entropy loss (increases in P_2 and $l_{b,eff}$). However, in the large strain region the entropy loss in the form of P_2 continues to increase, which mainly contributes to the enhanced mechanical properties.

We also studied the effects of architecture parameters (*i.e.* the length and number of graft chains) on the stress–strain behaviors of the blends at $\varepsilon_{RR} = 5.0$ and a strain rate of $0.2\tau^{-1}$. Two scenarios were proposed: one is to keep the whole number of polymer beads unchanged (that is 9000) while varying the length (from 3 to 6) and the number (from 6 to 3) of the graft chains in NR-*graft*-rigid-polymer molecules, and the results of this scenario are plotted in Fig. 6. In addition, we keep the number of molecules of each type (NR-*graft*-rigid-polymers and rigid polymers) invariable and set to be the same as the originals (180 rigid polymer molecules and 150 NR-*graft*-rigid-polymer molecules), as seen in Fig. S7 (ESI†).

As is seen in Fig. 6a and Fig. S7a (ESI†), the stress increases with increasing strain in both scenarios. However, in systems in which the NR-*graft*-rigid-polymer molecules have shorter graft chains, we find that the stress swiftly increases to a plateau at small strains and then changes little at large strains. Nearly the same values of stress have even been found at large strains in the systems in which the NR-*graft*-rigid-polymer molecules have identical lengths of graft chains. In comparison, in systems in which the NR-*graft*-rigid-polymer molecules have longer graft chains, the stress increases gradually at large strains, indicating that the increase in stress at large strains or the height of the curve is mostly governed by the length of the graft chains. Furthermore, at small strains, the stress in blends in which each NR-*graft*-rigid-polymer molecule has a greater number of graft chains rises significantly. This means that the increase in stress at small strains depends on the number of the graft chains.

The effective bond length and the change of nonbonding potential were calculated for blends with various structures.

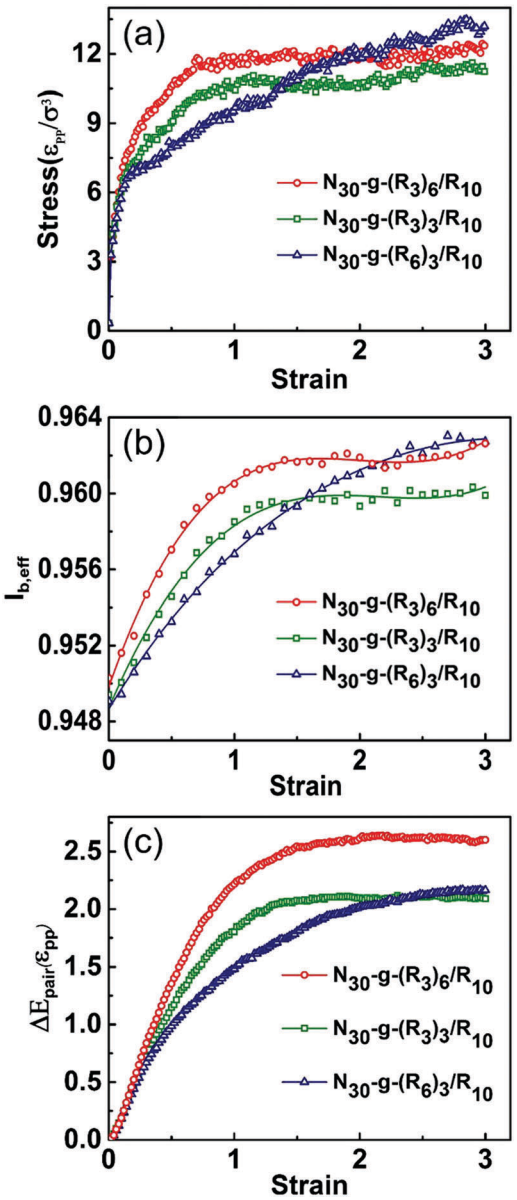

Fig. 6 (a) Stress–strain curves for various architecture parameters in systems of 9000 polymer beads ($(R_3)_6$ denotes 6 graft chains each with a length of 3). (b) Effective bond length $l_{b,eff}$ for various architecture parameters with respect to strain. (c) ΔE_{pair} as a function of strain for various architecture parameters.

As shown in Fig. 6b (for systems with a constant number (9000) of polymer beads), $l_{b,eff}$ increases rapidly at small strains. It then increases little at large strains in systems in which the NR-*graft*-rigid-polymer molecules have shorter graft chains, whereas larger values of $l_{b,eff}$ were found in systems in which the NR-*graft*-rigid-polymer molecules have more graft chains. However, there is a continuous increase in $l_{b,eff}$ at large strains in the systems in which the NR-*graft*-rigid-polymer molecules have longer graft chains, indicating that the greater increase in entropy loss in the form of $l_{b,eff}$ is mostly attributed to the number of graft chains at small strains and to the length of the

graft chains at large strains. The same trends of $l_{b,eff}$ were found for systems of a fixed molecular number (see Fig. S7c, ESI†). As for the bond orientation, which can be seen in Fig. S8 (ESI†), P_2 has almost the same value in different systems and shows increasing trends with increasing strain except for slight variations. Moreover, larger values of P_2 were found in systems in which the NR-*graft*-rigid-polymer molecules have longer graft chains at large strains, whereas for systems in which the NR-*graft*-rigid-polymer molecules have the same length of graft chains P_2 has a greater increase for molecules with a smaller number of graft chains. This means that systems in which the NR-*graft*-rigid-polymer molecules have fewer or longer graft chains exhibit a larger degree of bond orientation during the tensile process. Aside from entropy, the enthalpy in the form of ΔE_{pair} increases rapidly to a plateau as shown in Fig. 6c and Fig. S7d (ESI†). Obviously, the height of the curve is determined by the number of graft chains of the NR-*graft*-rigid-polymer molecules, and higher plateaus are reached during the tensile process in systems in which the NR-*graft*-rigid-polymer molecules have more graft chains, indicating that the contribution of enthalpy gain to the increase in stress is dominated by the number of graft chains. As for various structural systems, increases in both entropy loss (see Fig. 6b and Fig. S8, ESI†) and enthalpy gain (see Fig. 6c) contribute to the higher stress at small strains (see Fig. 6a), and a larger increase in entropy loss was found at large strains due to the sustained increase in $l_{b,eff}$ (see Fig. 6b), which causes the stress to rise (see Fig. 6a).

3.3. Comparison of N_{30}-*g*-$(R_3)_6/R_{10}$, N_{30} and N_{30}/R_{10}

In this subsection, we compare the mechanical properties of N_{30}-*g*-$(R_3)_6/R_{10}$ with those of N_{30} and N_{30}/R_{10}, and the stress–strain curves of these systems under uniaxial tension at a strain rate of $0.2\tau^{-1}$ are shown in Fig. 7a. Again, each system has the same number of polymer beads (9000 in total), while half of those are rigid, and ε_{RR} was fixed at 5.0.

As can be seen, both the N_{30}-*g*-$(R_3)_6/R_{10}$ and N_{30}/R_{10} blend systems exhibit enhanced mechanical properties compared to those of the neat polymer N_{30}, which becomes evident at large strains. However, nearly the same tensile behavior was found at small strains in both the N_{30}-*g*-$(R_3)_6/R_{10}$ and N_{30}/R_{10} blend systems (see Fig. 7b). This is reasonable since the two systems have similar physical states, which will be further discussed below. As the strain increases the difference in stress between the two blends becomes larger. The insets of Fig. 7c show the morphologies of the N_{30}-*g*-$(R_3)_6/R_{10}$ and N_{30}/R_{10} blends. A better compatibility of rigid polymer and NR was obtained in the N_{30}-*g*-$(R_3)_6/R_{10}$ blend, suggesting that the rigid polymer beads are better dispersed into the NR matrix because of the graft

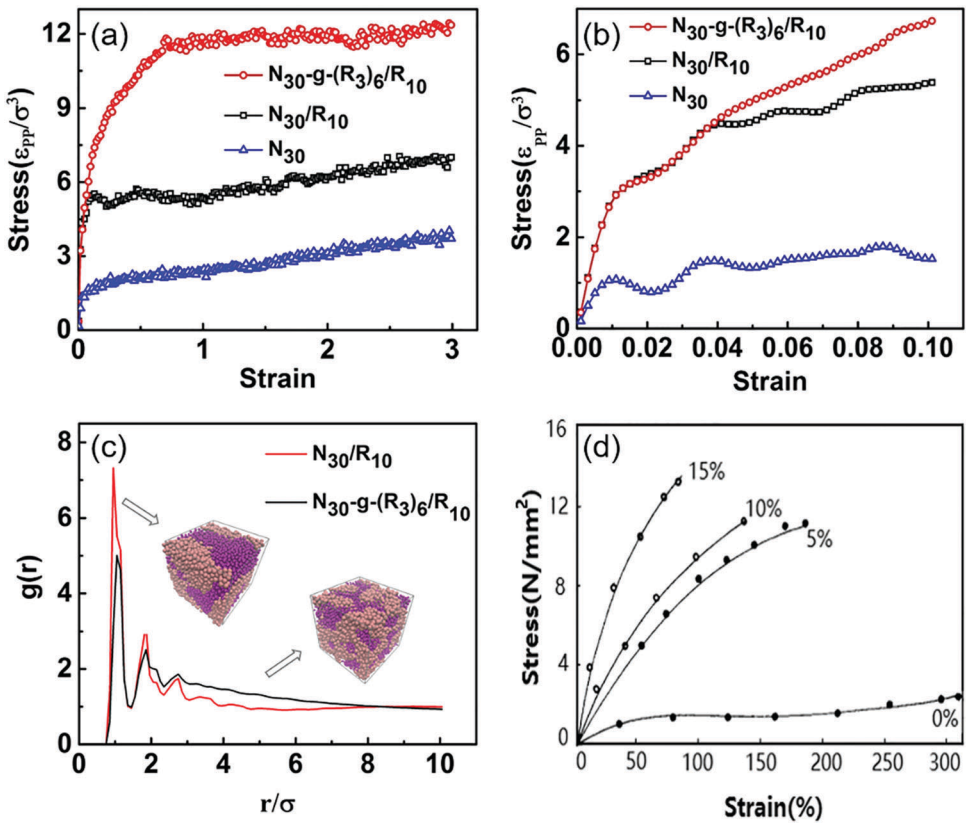

Fig. 7 (a) Stress–strain curves for the N_{30}-*g*-$(R_3)_6/R_{10}$, N_{30}/R_{10} and N_{30} systems. (b) Stress–strain curves at small deformations. (c) Radial distribution function *g*(*r*) between rigid polymer beads. (d) Stress–strain curve of NR/PMMA blends with and without the addition of graft copolymer (the ratio of the additional graft is shown beside the curves) and the mass ratio NR : PMMA = 1 : 1 from Oommen's experimental studies.[14] Reproduced from ref. 14 with permission from John Wiley and Sons, copyright 2004.

chains acting as a compatibilizer. However, the rigid polymer in the N_{30}/R_{10} blend is incompatible with the NR polymer, which also lowers the mechanical properties of the blend systems. These phenomena are in line with many experimental studies.[12–14] Fig. 7d is gathered from Oommen's experimental studies[14] and shows the stress–strain curve of 50/50 NR/PMMA blends with and without the addition of graft copolymer. Enhancement of the mechanical properties can be found by adding graft copolymer to the NR/PMMA blends, which supports our simulation results.

To characterize the compatibility and the interaction structure of the systems, the radial distribution function $g(r)$ between the rigid polymer beads was also calculated in Fig. 7c, which is defined as the probability of another rigid bead occurring from a distance of r,

$$g(r) = \frac{\langle n(r) \rangle}{4\pi r^2 \rho_0 \Delta r} \tag{7}$$

where $\langle n(r) \rangle$ is the average number of particles within the shell between r and $r + \Delta r$, Δr is a given thickness of spherical shell and ρ_0 is the entire number density of particles.[54] Zhuang *et al.*[55] found that $g(r)$ can provide promising evidence for evaluations of polymer compatibility. Xue *et al.*[56] found that the Flory–Huggins[57] parameter χ can evaluate the compatibility of the polymer blends. In that study it is shown that $g(r)$ and χ provide the same conclusions for the compatibility of the polymer blends.[56] The $g(r)$ also proves the better dispersion of rigid polymer beads in the N_{30}-g-$(R_3)_6/R_{10}$ blends. As shown in Fig. 7c, the peak intensity of the N_{30}-g-$(R_3)_6/R_{10}$ blends at $r = 3\sigma$ is smaller relative to that of the N_{30}/R_{10} blends, and the value of $g(r)$ is larger as r increases, suggesting that the average distance between rigid polymer beads is larger. In other words, the rigid polymer beads are well dispersed in the N_{30}-g-$(R_3)_6/R_{10}$ blend systems.

Obviously the value of P_2 becomes larger with increasing strain from Fig. 8a, which means the polymer chains transform from isotropic to anisotropic. The degree of bond orientation is smaller during the tensile process in the N_{30}/R_{10} blends than that in the N_{30}-g-$(R_3)_6/R_{10}$ blends, suggesting that the bonds are harder to orientate due to the greater effects of repulsiveness or incompatibility of the N_{30}/R_{10} blends. Fig. 8b shows that $l_{b,eff}$ increases gradually with increasing strain in the N_{30}-g-$(R_3)_6/R_{10}$ systems, whereas $l_{b,eff}$ barely increases in the N_{30} and N_{30}/R_{10} systems during the tensile process, indicating that the degree of bond stretching is larger in the N_{30}-g-$(R_3)_6/R_{10}$ systems than that in the N_{30}/R_{10} systems. The larger entropy loss of the N_{30}-g-$(R_3)_6/R_{10}$ blends originates from the greater increases in both P_2 and $l_{b,eff}$, which contributes to the enhanced mechanical properties. Moreover, the values of $l_{b,eff}$ in both blend systems are smaller than those in NR systems due to the stronger attraction between the rigid polymer beads. Additionally, in both blend systems ΔE_{pair} increases rapidly with increasing strain at small strains and then has small changes at large strains (see Fig. 8c), suggesting that the enthalpy gain in the form of an increase in ΔE_{pair} contributes to the increase in stress mostly at small strains. Furthermore, the values of ΔE_{pair} as well as $l_{b,eff}$ barely change during the whole tensile process in NR systems. This result indicates that the weak

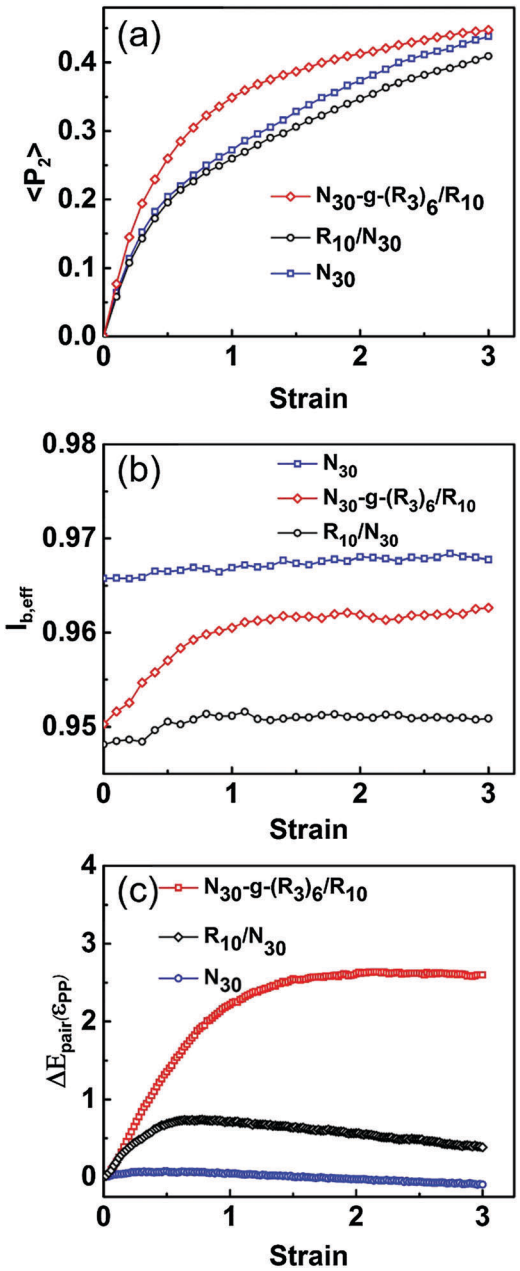

Fig. 8 (a) Bond orientation P_2 as a function of strain for the N_{30}-g-$(R_3)_6/R_{10}$, N_{30}/R_{10} and N_{30} systems. (b) Effective bond length $l_{b,eff}$ with respect to strain for the N_{30}-g-$(R_3)_6/R_{10}$, N_{30}/R_{10} and N_{30} systems. (c) ΔE_{pair} as a function of strain for the N_{30}-g-$(R_3)_6/R_{10}$, N_{30}/R_{10} and N_{30} systems.

mechanical properties of NR derive from lower increases in both entropy loss and enthalpy gain.

In Fig. 7b, the tensile behaviors of both the N_{30}-g-$(R_3)_6/R_{10}$ and N_{30}/R_{10} blends are nearly the same at the beginning, and the mechanical properties of both blend systems outperform those of the NR systems due to the addition of rigid polymers. The tensile processes start with energy-equilibrated systems, in which the polymer beads try to find the appropriate position to obtain a minimal energy. Moreover both blend systems have the same number and interaction potentials of the polymer beads, which results in almost the same changes in the bond

orientations and the nonbonding potential at small strains, as shown in Fig. 8a and c. As for the effective bond length, Fig. S9 (ESI†) shows that the changes of $l_{b,eff}$ for the two systems at small strains (<0.04) are close, which leads to a similar stress–strain behavior. With an increase in strain, the stress increases evidently in the N_{30}-*g*-$(R_3)_6/R_{10}$ systems, which exhibit enhanced mechanical properties in line with many experimental studies.[11,14] With contributions from both entropy loss and enthalpy gain, the stress increases during the tensile process. Furthermore, the nonbonding potential has no evident change at large strains (see Fig. 8c), while the value of P_2 is still rising, indicating that the contribution to the entropy loss is dominated by the bond orientation at large strains.

3.4. Comparison with experimental observations

This study has shown that additional NR-*graft*-rigid-polymers enhance the mechanical properties of pure NR systems and NR/rigid-polymer blend systems. There are some available experimental observations in the literature supporting our theoretical results. For instance, Oommen and coauthors have studied the effect of the concentration of NR graft PMMA (NR-*g*-PMMA) on the mechanical properties of NR/PMMA/NR-*g*-PMMA blends.[14] They found that systems without NR-*g*-PMMA possess a very low value of stress, while the addition of NR-*g*-PMMA considerably changes the nature of the stress–strain curve. In systems with higher concentrations of NR-*g*-PMMA higher values of stress were observed (see Fig. 7d) and other mechanical properties such as tensile moduli were also found to be enhanced. Moreover, better surface compatibility of NR and PMMA by addition of NR-*g*-PMMA was also found. This evidence is in good agreement with our simulation results. For example, the blend of NR-*graft*-rigid-polymer and rigid polymer has a higher value of stress relative to the blend of NR and rigid polymer (see Fig. 7a), and better compatibility of rigid polymer and NR was obtained in the N_{30}-*g*-$(R_3)_6/R_{10}$ blends from the morphologies in Fig. 7c.

Additionally, our simulation results reveal that the tensile modulus and stress can be enhanced by increasing the proportion of the rigid polymer (see Fig. 5a and Fig. S6a, ESI†). This result is in accordance with some experimental results. For example, Kovuttikulrangsie and coauthors studied the mechanical properties of poly(methyl methacrylate)-*grafted*-deproteinized natural rubber (PMMA-*g*-DPNR).[58] They found that by increasing the PMMA fraction in the PMMA-*g*-DPNR film, the tensile modulus and the tensile strength of the film were also increased, which is also in line with Neilsen's studies.[59] Jayasuriya's group investigated the mechanical properties of natural rubber/poly(methyl methacrylate) blends.[11] They found that the tensile strength and the modulus were increased significantly with increasing PMMA content. Moreover, some experimental studies, such as the study of Oommen[14] or the study of Thiraphattaraphun,[13] show that a higher graft ratio in the blend systems results in enhanced mechanical properties such as stress and modulus. These results are in line with our study on the structural factors. As the graft molecule in the blend systems changes from N_{30}-*g*-$(R_3)_3$ to N_{30}-*g*-$(R_6)_6$, namely increasing the length and number of graft chains in a molecule, a higher graft ratio and enhanced mechanical properties are obtained (see Fig. S7a, ESI†).

Beyond the reproductions of the general features of experimental findings for the blend of NR-*graft*-rigid-polymer and rigid polymer, the simulations can reveal the physical origin of the mechanical properties of the systems and provide an insight into the experimental observations. In the simulations it is convenient to visualize the morphology and to obtain molecular information. For instance, the morphologies of N_{30}-*g*-$(R_3)_6/R_{10}$ and N_{30}/R_{10} are shown in Fig. 7c. Better compatibility of rigid polymer and NR can be seen in the N_{30}-*g*-$(R_3)_6/R_{10}$ systems, indicating that the rigid polymer beads are well dispersed in the NR matrix because the graft chains act as a compatibilizer, which is also in line with Ekvipoo's studies.[60] More importantly, the dispersion state of the blends can be characterized easily by the radial distribution function $g(r)$ between the rigid polymer beads. The rigid polymer beads are well dispersed as reflected by the smaller peak of the N_{30}-*g*-$(R_3)_6/R_{10}$ blends appearing at $r = 3\sigma$ and displaying a larger $g(r)$ when r increased (see Fig. 7c). Moreover, it is facile to calculate dynamic parameters which can reveal the microscopic origin of the enhanced mechanical properties in the blend systems. For example, the contribution to the enhanced systems in terms of conformational entropy can be easily elucidated by the bond orientation and the effective bond length. The contribution from the view of interaction enthalpy can be explained by the change of nonbonding potential.[22] Such dynamic parameters reveal the physical origin and deepen the understanding of experimental observations. This is of practical benefit for experimentally designing and fabricating advanced materials.

4. Conclusions

By changing an external factor (the strain rate) and internal factors such as nonbonding interaction strength, architectural structures (the length and number of graft chains of the NR-*graft*-rigid-polymer molecules) and the proportion of rigid polymer, we investigate the mechanical properties of NR-*graft*-rigid-polymer/rigid-polymer systems (N_{30}-*g*-$(R_3)_6/R_{10}$) using molecular dynamics simulation. It is found that N_{30}-*g*-$(R_3)_6/R_{10}$ systems with a higher strain rate exhibit a better mechanical performance, such as a higher yield stress or modulus. As for the effects of internal factors on the mechanical properties of the N_{30}-*g*-$(R_3)_6/R_{10}$ systems, the stress and modulus were found to be increased by increasing the nonbonding interaction strength between rigid polymers. However, as the rigid polymer proportion increases in the systems, as mechanical properties tend to be governed by the rigid polymers, the tensional modulus increases gradually but the flexibility of the systems is reduced due to the reduction in soft NR parts. Moreover, the stress will increase to a limit as the rigid part increases, which means that significantly enhanced tensile properties are not obtained when the proportion of additional rigid polymer is more than about 75%. In addition, a larger stress and modulus were found at small strains in systems in which NR-*graft*-rigid-

polymer molecules had more graft chains. Nevertheless, a continuous increase in stress was found at large strains in systems in which NR-*graft*-rigid-polymer molecules had longer graft chains. Moreover, we compared the blend of NR-*graft*-rigid-polymer and rigid polymer (N_{30}-*g*-$(R_3)_6/R_{10}$) with the blend of NR and rigid-polymer (N_{30}/R_{10}) and neat NR (N_{30}), and found that N_{30}-*g*-$(R_3)_6/R_{10}$ exhibits enhanced mechanical properties over N_{30}/R_{10} and N_{30}, and in addition a better dispersion of rigid polymer was found in N_{30}-*g*-$(R_3)_6/R_{10}$. These results are also in qualitative accordance with available experimental observations. Lastly, comparisons were made to provide the rationality of our models. The effects of these parameters on the mechanical properties were found to be in connection with the bond orientation, the effective bond length, and the change of nonbonding potential. Insight into various mechanical properties of the N_{30}-*g*-$(R_3)_6/R_{10}$ systems is obtained, which may help us to find useful information for designing and fabricating high performance NR materials.

Conflicts of interest

There are no conflicts to declare.

Acknowledgements

This research was supported by the Fundamental Research Funds for the Central Universities of China (22A201514002), the Shanghai Leading Academic Discipline Project (No. B502), and the Shanghai Key Laboratory Project (No. 08DZ2230500).

Notes and references

1 M. M. Rippel, C. A. P. Leite and F. Galembeck, *Anal. Chem.*, 2002, **74**, 2541–2546.
2 P. Piya-areetham, G. L. Rempel and P. Prasassarakich, *Polym. Degrad. Stab.*, 2014, **102**, 112–121.
3 A. T. Koshy, B. Kuriakose, S. Thomas and S. Varghese, *Polymer*, 1993, **34**, 3428–3436.
4 N. Hayeemasae, H. Ismail and A. R. Azura, *Polym.-Plast. Technol. Eng.*, 2013, **52**, 501–509.
5 S. Chattopadhyay and S. Sivaram, *Polym. Int.*, 2001, **50**, 67–75.
6 C. C. Ho, M. C. Khew and Y. F. Liew, *Surf. Interface Anal.*, 2001, **32**, 133–143.
7 P. Akcora, S. K. Kumar, V. G. Sakai, Y. Li, B. C. Benicewicz and L. S. Schadler, *Macromolecules*, 2010, **43**, 8275–8281.
8 K. Yang and M. Gu, *Polym. Eng. Sci.*, 2009, **49**, 2158–2167.
9 N. R. Manoj and P. P. De, *Polymer*, 1998, **39**, 733–741.
10 L. Lin, C. M. Chan and L. T. Weng, *Polymer*, 1998, **39**, 2355–2360.
11 M. M. Jayasuriya and D. J. Hourston, *J. Appl. Polym. Sci.*, 2012, **124**, 3558–3564.
12 R. Stephen, C. Ranganathaiah, S. Varghese, K. Joseph and S. Thomas, *Polymer*, 2006, **47**, 858–870.
13 L. Thiraphattaraphun, S. Kiatkamjornwong, P. Prasassarakich and S. Damronglerd, *J. Appl. Polym. Sci.*, 2001, **81**, 428–439.
14 Z. Oommen, M. R. G. Nair and S. Thomas, *Polym. Eng. Sci.*, 1996, **36**, 151–160.
15 C. Nakason, Y. Panklieng and A. Kaesaman, *J. Appl. Polym. Sci.*, 2004, **92**, 3561–3572.
16 J. L. Collins and A. D. T. Gorton, *NR Technol.*, 1984, **15**, 69–77.
17 A. D. T. Gorton, *NR Technol.*, 1984, **15**, 7–18.
18 J. D. Anderson, *Computational Fluid Dynamics: The Basic with Application*, McGraw-Hill, New York, 1995.
19 S. Chen and G. D. Doolen, *Annu. Rev. Fluid Mech.*, 1998, **30**, 329–364.
20 G. D. Smith and D. Bedrov, *Langmuir*, 2009, **25**, 11239–11243.
21 J. Shen, J. Liu, Y. Gao, D. Cao and L. Zhang, *Langmuir*, 2011, **27**, 15213–15222.
22 T. Jiang, L. Wang and J. Lin, *RSC Adv.*, 2014, **4**, 35272–35283.
23 A. Adnan, C. T. Sun and H. Mahfuz, *Compos. Sci. Technol.*, 2007, **67**, 348–356.
24 O. Borodin, D. Bedrov, G. D. Smith, J. Nairn and S. Bardenhagen, *J. Polym. Sci., Part B: Polym. Phys.*, 2005, **43**, 1005–1013.
25 J. Cho and C. T. Sun, *Comput. Mater. Sci.*, 2007, **41**, 54–62.
26 J. Liu, S. Wu, L. Zhang, W. Wang and D. Cao, *Phys. Chem. Chem. Phys.*, 2011, **13**, 518–529.
27 P. R. Mantena, A. Al-Ostaz and A. H. D. Cheng, *Compos. Sci. Technol.*, 2009, **69**, 772–779.
28 A. Kutvonen, G. Rossi, S. R. Puisto, N. K. Rostedt and T. Ala-Nissila, *J. Chem. Phys.*, 2012, **137**, 214901.
29 S. Y. Fu, X. Q. Feng, B. Lauke and Y. W. Mai, *Composites, Part B*, 2008, **39**, 933–961.
30 S. T. Knauert, J. F. Douglas and F. W. Starr, *J. Polym. Sci., Part B: Polym. Phys.*, 2007, **45**, 1882–1897.
31 J. Xiao, Y. Huang, Y. Hu and H. Xiao, *Sci. China: Chem.*, 2005, **48**, 504–510.
32 J. Liu, S. Wu, L. Zhang, W. Wang and D. Cao, *Phys. Chem. Chem. Phys.*, 2011, **13**, 518–529.
33 J. I. Kroschwitz, *Concise Encyclopedia of Polymer Science and Engineering*, Wiley, London, 1990.
34 R. E. Rudd and J. Q. Broughton, *Phys. Rev. B: Condens. Matter Mater. Phys.*, 1998, **58**, R5893–R5896.
35 M. P. Allen and D. J. Tildesley, *Computer Simulation of Liquids*, Clarendon Press, Oxford, 1987.
36 Q. Wang, D. J. Keffer, D. M. Nicholson and J. B. Thomas, *Macromolecules*, 2010, **43**, 10722–10734.
37 L. M. Dupuy, E. B. Tadmor, R. E. Miller and R. Phillips, *Phys. Rev. Lett.*, 2005, **95**, 060202.
38 S. Sen, S. K. Kumar and P. Keblinski, *Macromolecules*, 2005, **38**, 650–653.
39 F. Lahmar, C. Tzoumanekas, D. N. Theodorou and B. Rousseau, *Macromolecules*, 2009, **42**, 7485–7494.
40 L. J. Chen, H. J. Qian, Z. Y. Lu, Z. S. Li and C. C. Sun, *J. Phys. Chem. B*, 2006, **110**, 24093–24100.
41 C. Bennemann, W. Paul, J. Baschnagel and K. Binder, *J. Phys.: Condens. Matter*, 1999, **11**, 2179–2192.
42 S. L. Lin, N. Numasawa, T. Nose and J. P. Lin, *Macromolecules*, 2007, **40**, 1684–1692.

43 J. Liu, Y. Wu, J. Shen, Y. Gao, L. Zhang and D. Cao, *Phys. Chem. Chem. Phys.*, 2011, **13**, 13058–13069.
44 K. Kremer and G. S. Grest, *J. Chem. Phys.*, 1991, **94**, 4103.
45 S. Plimpton, *J. Comput. Phys.*, 1995, **117**, 1–19.
46 K. Kremer and G. S. Grest, *J. Chem. Phys.*, 1990, **92**, 5057–5086.
47 P. Xu, J. Lin and L. Zhang, *J. Phys. Chem. C*, 2017, **121**, 28194–28203.
48 J. Liu, Y. Gao, D. Cao, L. Zhang and Z. Guo, *Langmuir*, 2011, **27**, 7926–7933.
49 J. E. Mark, *Polymer Data Handbook*, Oxford University Press, Oxford, 2009.
50 J. Gao and J. H. Weiner, *J. Chem. Phys.*, 1995, **103**, 1614–1620.
51 D. R. Rottach, J. G. Curro, G. S. Grest and A. P. Thompson, *Macromolecules*, 2004, **37**, 5468–5473.
52 L. Zhang, J. Lin and S. Lin, *Soft Matter*, 2009, **5**, 173–181.
53 X. Zhu, L. Wang and J. Lin, *Macromolecules*, 2011, **44**, 8314–8323.
54 S. S. Jawalkar, K. V. Raju, S. B. Halligudi, M. Sairam and T. M. Aminabhavi, *J. Phys. Chem. B*, 2007, **111**, 2431–2439.
55 Q. X. Zhuang, Z. J. Xue, X. Y. Liu, Y. L. Yuan and Z. W. Han, *Polym. Compos.*, 2011, **32**, 1671–1680.
56 Z. J. Xue, X. Y. Liu, Q. X. Zhuang, K. Hu and Z. W. Han, *Polym. Compos.*, 2012, **33**, 430–435.
57 P. G. De Gennes, *Scaling Concepts in Polymer Physics*, Cornell University Press, Ithaca, 1979.
58 S. Kovuttikulrangsie, K. Sahakaro, C. Intarakong and P. Klinpituksa, *J. Appl. Polym. Sci.*, 2004, **93**, 833–844.
59 L. E. Nielsen and R. F. Landel, *Mechanical Properties of Polymers and Composites*, Reinhold, New York, 1974.
60 K. Ekvipoo, V. Norbert, K. Claudia and N. Charoen, *Iran. Polym. J.*, 2012, **21**, 689–700.

